Analysis of Transient Fault Currents in Multi-Terminal HVDC Networks during Pole-to-Ground Faults

Matthias K. Bucher, Christian M. Franck

***Abstract*– The fault current development in a circuit breaker during a pole-to-ground fault is analyzed for a generic multi-terminal HVDC system based on Voltage Source Converters. The paper aims to contribute to the current discussion of which requirements on breaking time and peak current HVDC circuit breakers need to fulfill in such networks either based on OHLs or cables. Therefore, the fault current is broken down into the individual contributions of the different network components and their influence on the development of the fault current in the circuit breaker of the faulted line is illustrated. In doing so, the emphasis is on the comparison of the sensitivities in cable and OHL systems.**

***Keywords*: HVDC transmission, Power system faults, Power system simulation, PSCAD.**

I. Introduction

THE growing electricity demand, the increasing deployment of decentralized renewable energy sources, and the resulting long transmission distances between the generation and the load centers pose some major challenges to the electrical power network. The existing grid has reached its capability limit in various regions of the world and an expansion is indispensable. A network based on AC transmission technology is, however, not economical for very long transmission distances. The Multi-Terminal HVDC (MTDC) network is a promising alternative and has become a viable option due to advances in the HVDC technology such as higher ratings of the semiconductor devices and the development of Voltage Source Converters (VSC). Increased system redundancy, higher flexibility for power trading, and reduced investment and operational costs are expected benefits of an interconnected HVDC power network. Such a network can be applied as an overlay grid to reinforce the existing transmission capacities of the AC network, e.g. Pan-European Supergrid, to interconnect different AC systems with large offshore wind parks e.g. in the North Sea [1]–[5] and on the US east coast [6], or to connect solar power plants in Northern Africa to the load centers in Europe, as proposed in the DESERTEC initiative [7].

Grid protection is currently one of the main difficulties of MTDC networks. For the reliable breaking of DC fault currents and the selective isolation of faulted lines, DC circuit breakers (CBs) are indispensable. Conventional AC side CBs provide adequate protection for point-to-point HVDC connections, but would not be viable for HVDC grids, as they require the de-energization of the entire system [8], [9]. There exist several concepts for DC CBs [10], [11], [2], which still have to be improved in terms of on-state losses or breaking time before they can be of practical use. Other concepts to address fault clearance have to be chosen as long as no fully satisfying DC CB concept is developed [12].

This paper aims to contribute to a better understanding of the transient development of the fault current through a DC CB during a pole-to-ground fault in a multi-terminal VSC HVDC network. Therefore, the fault current is broken down into individual contributions of the different network components, a concept which has been introduced in [13] for a submarine cable MTDC. The fault current contributing system components are the DC capacitors, overhead lines (OHLs) or cables, and the adjacent AC network. A breakdown of the fault current allows for a detailed analysis of the influence of the component parameters and fault condition on the total fault current in the DC CB. It enables the specification of DC CB requirements and fault detection mechanisms, as well as the identification of measures to reduce the transient overcurrent. In addition to [13], the paper at hand compares the results of the cable system with those of an OHL system. It illustrates the sensitivities of the key parameters in different scenarios, which consider the transmission technology, i.e. OHL or cable, the converter technology including the required DC filters, and the fault condition.

To do so, simulations in PSCAD-EMTDC of pole-to-ground faults in a simple, bipolar, radial three-terminal HVDC system are performed and analyzed. This is the simplest possible layout including all available components, which are able to contribute to the fault current in the CB. The emphasis in this paper is on pole-to-ground faults, since they are regarded as significantly more frequent compared to pole-to-pole faults [14], although the latter fault would lead to more severe conditions [15].

The paper is structured as follows: Section II describes the temporal development of the transient currents and voltages during a pole-to-ground fault and Section III explains the methodology of transient simulations. Section IV presents the results of the simulations followed by the conclusion in Section V.

The project is financially supported by ABB Switzerland Ltd, Siemens AG, Alstom Grid, and the Swiss Federal Office of Energy (BfE).

M. K. Bucher and C. M. Franck are with the Power Systems and High Voltage Laboratories, ETH Zurich, 8092 Zurich, Switzerland (e-mail: bucher, franck@eeh.ee.ethz.ch).

Paper submitted to the International Conference on Power Systems Transients (IPST2013) in Vancouver, Canada July 18-20, 2013.

II. Pole-to-Ground Faults

Pole-to-ground faults in cable systems are less frequent than in OHL networks, but are often permanent and require repairing the affected cable. Aging of the cable's main insulation or external damages due to digging or anchoring in case of sea cables [16] may lead to a breakdown of the cable insulation and a pole-to-sheath fault, which develops into a pole-to-ground fault. In OHL systems, a pole-to-ground fault can be provoked by a lightning strike and subsequent back-flashover to the supporting tower or direct touching of the conductor to an external object, e.g. a tree.

In both cases, cable and OHL lines, the voltage at the fault location decreases within a few microseconds after the fault occurs to a level given by the fault resistance. Its value depends on the magnitude of the fault current and the characteristics of the soil, e.g. the ionization and de-ionization time constants, and the soil resistivity, as described in [17]. Additionally, the tower footing resistance has to be added in case of a tower back-flashover in OHL systems. A cable pole-to-ground fault impedance includes initially the sheath impedance between the fault location and the next grounding point of the sheath. The increasing current through the sheath will most probably lead to an explosion and destruction of the cable at the fault location resulting in a direct, low-ohmic path from the conductor to the ground. The voltage drop at the fault location occurs very quickly, but not instantaneously due to the voltage supporting, distributed line capacitance and the inductance in the fault path. In general, the higher the fault resistance, the lower the voltage drop along the line. Right after the fault occurrence, negative voltage surges start to travel from the fault location into both directions towards the terminals. Along its way, the distributed line capacitance is discharged gradually into the ground fault.

Upon the arrival at the terminals after the traveling time τ, the negative voltage surge is reflected back as a positive surge due to the capacitive termination of the cable given by the DC capacitors [18], [19]. Depending on the converter technology, VSC capacitors and filter capacitors are required at the DC side of a VSC in order to reduce the voltage ripple, which is injected by the converter. A 3-level neutral point clamped VSC requires less filering, but an about three times higher capacitor volume than a 2-level topology for the same target value of less than 5% voltage ripple on the DC line [20]. This is mainly due to a lower switching frequency used in the multi-level topologies. Other topologies such as the Modular Multi-level Converter (MMC) [21] with a sufficiently large number of submodules do not need any additional filtering on the DC side and the storage capacitors cannot be discharged during a DC pole-to-ground fault while the converter valves are blocked [22] as shown in Fig. 1. To provide a reference voltage in bipolar HVDC schemes, the midpoint of the capacitors is usually grounded [23], [20] either via a low-ohmic connection or a reactor. The grounded capacitor midpoint and the ground fault form a loop that provokes a discharge of the capacitors. Low-ohmic grounding allows for monopolar operation of the bipole, but results in high ground currents, whereas the grounding via reactor suppresses such currents, but disables the monopolar operation option.

The discharge current of the capacitor is then superposed on the reflected, backward traveling current surge, which can be approximated by the convolution of the incident wave form and the impulse response of the filter [24]. As the reflected surge arrives again at the fault location, one part is reflected and the other part transmitted through the fault into the opposite section of the line according to the reflection coefficient Γ and transmission coefficient T. The resulting forward and backward traveling surges yield multiple capacitor discharge peaks.

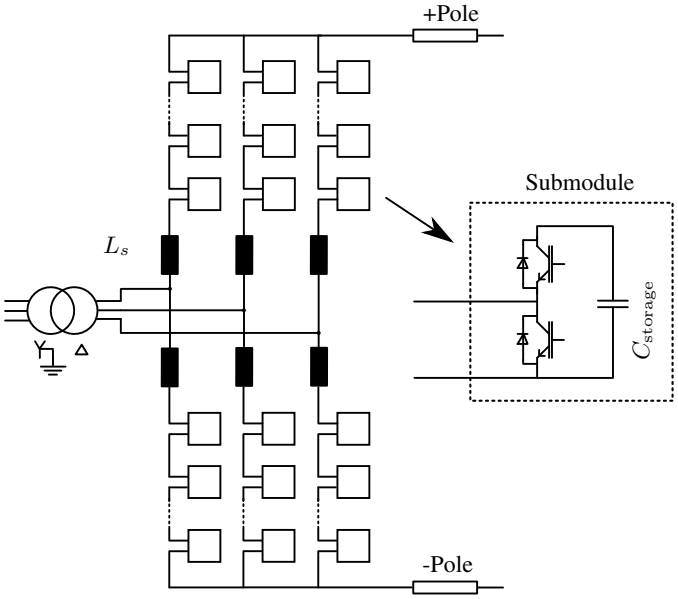

Fig. 1. MMC topology

III. Method

This section describes the model of the overall grid layout, the converter model, the cable model, and the OHL model.

A. Network and Converter Model

The 3 terminal radial HVDC grid with either cable or OHL interconnections shown in Fig. 2 is modeled in PSCAD using the EMTP approach [25]. A pole-to-ground fault with a fault resistance R_{f} is applied $100\,\text{km}$ away from terminal 1. The converters are modeled as $\pm 320\,\text{kV}$ $900\,\text{MW}$ bipolar two-level VSC converters with concentrated midpoint-grounded DC capacitors at each terminal as depicted in Fig. 3. The capacitive coupling of the positive and negative pole, which may induce voltage surges on the healthy pole [19], [18], is neglected. In case of interconnections with screened cables, this is a justified simplification, whereas in OHL links, the distance between the poles has to be large enough to ensure that the induced voltage step is negligibly small. Applying this assumption, the bipole can be simplified to an asymmetrical monopole, which is equally valid to a bipole without coupling of the poles. After detection of the fault, the control in a real converter protects the Insulated Gate Bipolar Transistor (IGBT) modules from overcurrents through blocking of the

valves within a few μs making the half-bridge based VSC an uncontrolled rectifier [26], [27]. The PSCAD implementation of the converters used in this study consists of a constant voltage source for the initial steady-state operation and a transient model comprising the freewheeling diodes only as illustrated in Fig. 4. No implementation of IGBTs or switching control is required in this transient study. At the beginning of the simulation, the system is in steady-state operation. The values of the constant voltage sources at each terminal are set in order to reach approximately the nominal line currents i_{12} and i_{13} of $0.5\,\mathrm{p.u.}$ assuming that terminal 1 is operated in rectifier mode and terminals 2 and 3 are operated as inverters. The fault is detected independently at each terminal by measuring the di/dt of the line current. In contrast to the overcurrent detection in the converter valves, fault detection at the feeder allows a faster blocking of the IGBTs. The threshold of detection is set to a small value of $1.5 \cdot 10^{-6}\,\mathrm{kA}/\mu\mathrm{s}$, at which the converter model is switched to the transient model through opening of BRK 1 and closing of BRK 2 (c.f. Fig. 4). The adjacent AC networks are modeled by their equivalent short-circuit impedance consisting of R_{AC} and L_{AC}, and a voltage source V_{AC}. The primary windings of the converter transformers have star configuration with grounded neutral and delta configuration on the secondary side. The additional phase reactor L_{s} between the converter bridge and the transformer serves for harmonic filtering of the AC currents. The values of system parameters are summarized in Table I. The losses of the transient converter model during the AC infeed are determined by the on-state resistance R_{D} of the freewheeling diodes. The value for R_{D} is based on a series connection of 89 $4500\,\mathrm{kV}/2000\,\mathrm{A}$ press-pack IGBTs [28]. Terminal 1 is operated in rectifier mode and terminals 2 and 3 are operated as inverters with a secondary winding voltage of each converter transformer of $213\,\mathrm{kV}$.

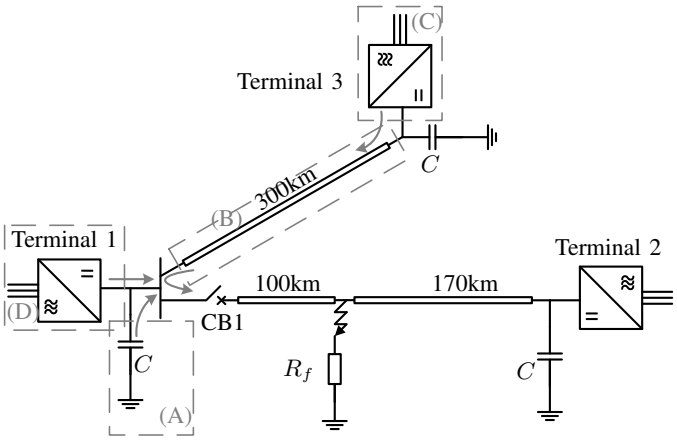

Fig. 2. Network layout with different fault feeding sources: (A) filter capacitor, (B) adjacent feeder cable, (C) AC infeed at terminal 3, (D) AC infeed at terminal 1

B. Cable Model

The cable model makes use of the EMTDC detailed frequency dependent, distributed-parameter model. The general design of the cable cross-section is derived from a real $150\,\mathrm{kV}$ XLPE VSC-HVDC submarine cable [29], [16]. The cross-section was scaled up to a $320\,\mathrm{kV}$ cable respecting the diameter of the copper conductor [30], while keeping the electric field stress similar. The material properties are based on values given in [31]. The cable cross-section dimensions and material properties are summarized in Table II [12].

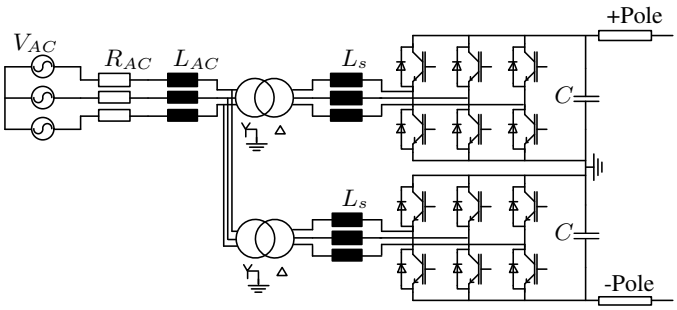

Fig. 3. Scheme of the converter model (V_{AC}: AC voltage, R_{AC}: AC resistance, L_{AC}: AC inductance, L_{s}: phase reactor, C: DC filter capacitor)

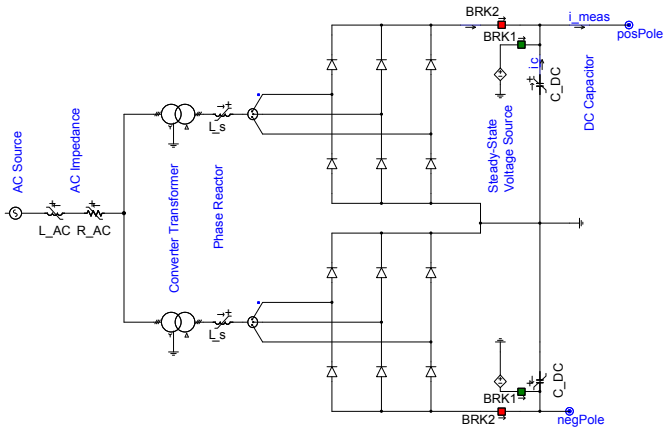

Fig. 4. PSCAD converter model

C. OHL Model

The implemented OHL model is based on real data of a HVDC OHL connection. The parameters of the stranded 45/7 AL3/Steel conductors and steel shield wires are taken from the IEC technical report 61597 for OHLs [32]. The monopolar tower dimensions are based on data of the $500\,\mathrm{kV}$ Inga-Shaba HVDC link [33]. The OHL properties are summarized in Table III. The selected conductors of the OHL have a similar current carrying capacity as compared with the XLPE cable, whereas the rated voltage is much higher. For better comparison of

TABLE I
SYSTEM PARAMETERS

Parameter	Value
Rated Converter Power (Bipole)	$900\,\mathrm{MW}$
DC Voltage	$\pm 320\,\mathrm{kV}$
AC Voltage (L-L, RMS)	$400\,\mathrm{kV}$
X/R of AC Network	10
Transformer Secondary Winding Voltage	$213\,\mathrm{kV}$
Transformer Leakage Reactance	$0.1\,\mathrm{p.u.}$
Converter Phase Reactor	$0.05\,\mathrm{p.u.}$
Total Resistance of Converter Diodes	$0.1691\,\Omega$

TABLE II
PROPERTIES OF THE ASSUMED 320 kV XLPE CABLE [12]

Layer	Material	Outer Radius (mm)	Resistivity (Ωm)	Rel. permittivity	Rel. permeability
Core	Copper	21.4	$1.72 \cdot 10^{-8}$	1	1
Insulation	XLPE	45.9 [1]	-	2.3	1
Sheath	Lead	49.4	$2.2 \cdot 10^{-7}$	1	1
Insulation	XLPE	52.4	-	2.3	1
Armor	Steel	57.9	$1.8 \cdot 10^{-7}$	1	10
Insulation	PP	61.0	-	2.1	1

[1] Including inner and outer semi-conductor layer of 1.2 and 1.3 mm thickness, respectively

TABLE III
PROPERTIES OF THE 500 kV OHL

Parameter	Value
Conductor Radius	16.2 mm
Strand Radius	4.5 mm
Total # of Strands	52
# of Outer Strands	21
Sag	13.9 m
Height of Conductor	25.32 m

the simulation results of the two transmission media, the rated voltage of the OHL is reduced to the cable voltage of 320 kV and the same converter ratings as in the cable system are applied.

IV. RESULTS AND DISCUSSION

Simulations have been performed using a time step of 10 μs. The DC capacitor size, the fault resistance, and the short circuit ratio (SCR) at the point of common coupling (PCC) are varied using both transmission technologies. A comparison of the parameter sensitivities of OHL and cables is presented in the following paragraphs.

A. Comparison of Line Parameters

Table IV compares the line parameters of the cable and OHL at 0.001 Hz, which have been extracted using the PSCAD Line Constants Program. The longitudinal losses R, the transversal losses G, and the capacitance C of the two transmission technologies reveal the largest differences. The conductor in the cable has a larger cross section and is made of copper instead of aluminium/steel, which results in lower longitudinal losses compared with the OHL. The capacitance and the transversal losses of the cable, however, are two orders of magnitude larger than in the OHL due to the cable design with XLPE insulation and screen. The resulting propagation velocity of the quasi TEM-mode v_0 is about 100 % of the speed of light in the OHL and around 66 % in the cable. The traveling delays for 100 km are indicated by τ_{100km} for both transmission media. The indicator $\mu = 0.5 \cdot (\alpha + \beta)$ is a measure for the damping of the amplitude of a traveling wave introduced by the losses and $\nu = 0.5 \cdot (\alpha - \beta)$ is an indicator for the distortion of the wave shape. $\alpha = R/L$ is the inductive and $\beta = G/C$ the capacitive damping factor as defined in [24]. The OHL exhibits a higher damping, but less distortion of the wave shape, i.e. the wave fronts are not flattened as much as in the cable. For a distortionless transmission line, the Heaviside condition $\nu = 0$ has to be fulfilled [24].

TABLE IV
COMPARISON OF OHL VS. CABLE PARAMETERS AT 1 mHz

Parameter	OHL	Cable
$R[\Omega/km]$	0.0578	0.0123
$X[\Omega/km]$	$2.03 \cdot 10^{-5}$	$2.17 \cdot 10^{-5}$
$G[S/km]$	$1.0 \cdot 10^{-8}$	$1.0 \cdot 10^{-6}$
$B[S/km]$	$5.29 \cdot 10^{-11}$	$1.18 \cdot 10^{-9}$
$v_0[km/s]$	$3.0 \cdot 10^{5}$	$1.98 \cdot 10^{5}$
$\tau_{100km}[ms]$	0.33	0.5
μ	9.56	4.44
ν	8.37	-0.87

B. Base Case

The base case assumes a constant fault resistance of 5 Ω, DC capacitors of 50 μF at each terminal, and an SCR of the AC system at each PCC of 20. The SCR is defined as the ratio of the short circuit capacity at the PCC and the rated power of the converter as follows:

$$\text{SCR} = S^{\text{sc}}_{\text{PCC}} / S^{\text{rated}}_{\text{converter}} \quad . \tag{1}$$

Fig. 5 illustrates the simulation results of the base case for a cable system (upper graph) and OHL system (lower graph). The plots show the superposition of the individual fault current contributions of the DC capacitor (A), the adjacent feeder capacitance and the filter capacitor at terminal 3 (B), the AC infeed at the remote terminal 3 (C), and the AC infeed at closest terminal 1 (D) (c.f. Fig. 2). The contributions (A) and (D) are determined easily by measuring the corresponding currents in the capacitor and at the output of the converter bridge, respectively. To determine the contributions from the neighboring feeder capacitance (B) and the remote terminal (C), however, the measured current at the receiving end of the adjacent feeder has to be further broken down based on two sequent simulations: first with terminal 3 connected to the system and second without terminal 3 (only with the filter capacitor connected to the remote end). No direct measurement of the AC infeed at terminal 3 (D) is possible due to the time delay and distortion introduced by the line connecting terminal 3 and 1. The pole-to-ground fault occurs at 0 ms. Discharge of concentrated DC capacitors and distributed feeder capacitance is dominant during the first 10 ms. Thereafter, the capacitive discharges fade out and the main fault current contributors are the infeed from the AC side at terminals 3 and 1. The DC capacitors are periodically charged by the AC infeed and discharged into the fault. Note that the negative current (capacitor charging) is truncated in Fig. 5, since it does not contribute to the CB current. During the second period after 10 ms, a 300 Hz ripple is visible that is injected from the converters acting as 6-pulse rectifiers. The main differences between cables and OHL are found in the maximum steady-state fault current in the CB after 100 ms, which is about 14 kA in the cable and about 11 kA in the OHL system for this base case. The maximum steady-state fault current is determined by the series line impedance and, therefore, the OHL connections, which have a higher impedance than

the cables, yield lower fault current values. Moreover, the capacitive discharge dominated first period exhibits a distinct behavior in the two transmission technologies: the cable is dominated by large discharge peaks with high di/dts from the DC filters, whereas the OHL connections lead to much smaller filter discharge peaks using the same filter size as in the cable system. Although the distortion of the negative voltage surges is lower in OHLs as compared to cables (c.f. Table IV) and one would expect higher dv/dts leading to larger capacitor discharge currents, the OHL yields lower capacitor current contributions than cables due to the larger damping in the system. The frequency of the subsequent discharges, however, is higher in the OHL given the higher surge propagation v_0 speed as compared to the cable (c.f. Table IV). Also the fault current contribution of the adjacent feeder at the bus at terminal 1 is much lower in the OHL system due to its relatively low capacitance.

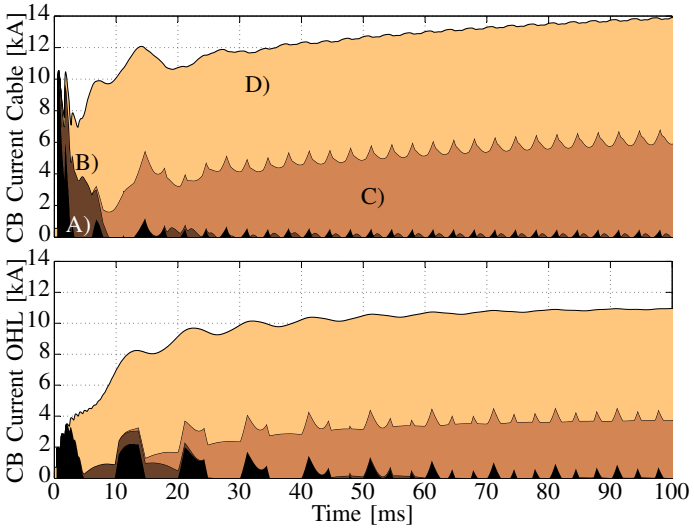

Fig. 5. Fault current contributions: (A) DC capacitor, (B) adjacent feeder cable, (C) AC infeed at terminal 3, (D) AC infeed at terminal 1

C. Influence of DC Capacitance

The size of the DC capacitor has been varied between $0.1\,\mu$F and $100\,\mu$F. The fault resistance is kept constant at $5\,\Omega$. Fig. 6 shows the fault current contributions during the first $10\,$ms after the ground fault has occurred for the lowest (upper row) and highest capacitor size (lower row) and the two transmission technologies: cable (left column) and OHL (right column). Generally, a change in the DC capacitor size has no impact on the steady-state fault current, but only on the first, capacitive discharge dominated period. In both, cables and OHLs, very small DC capacitors yield a negligibly small contribution to the overall fault current in the CB. In the case of cables, the first peak is dominated by the discharge of the distributed capacitance of the adjacent feeder cable to terminal 1. In OHLs, only the AC infeed at terminal 1 contributes to the CB current, which increases rather slowly due to the limiting AC impedance.

If large capacitors are installed, the cable exhibits the characteristic discharge pattern with a first peak from the initial negative voltage surge at $0.5\,$ms, a second peak at $1.5\,$ms from the second negative voltage surge, which corresponds to the reflected surge (reflected at the fault location), and a subsequent decrease in the capacitor current at $2.2\,$ms due to an incident positive voltage surge. This positive surge originated at terminal 2 from the incident initial negative surge and was then transmitted through the ground fault location to terminal 1. The following gradually decreasing peaks correspond to the subsequent arrivals of the surges at the terminal.

The OHL leads to a series of superposing small capacitor discharges. The maximum of the DC capacitor contribution occurs later at around $3\,$ms and is smaller than in the cable. Generally, a change in the capacitor size has less influence on the CB current development in the OHL than in the cable.

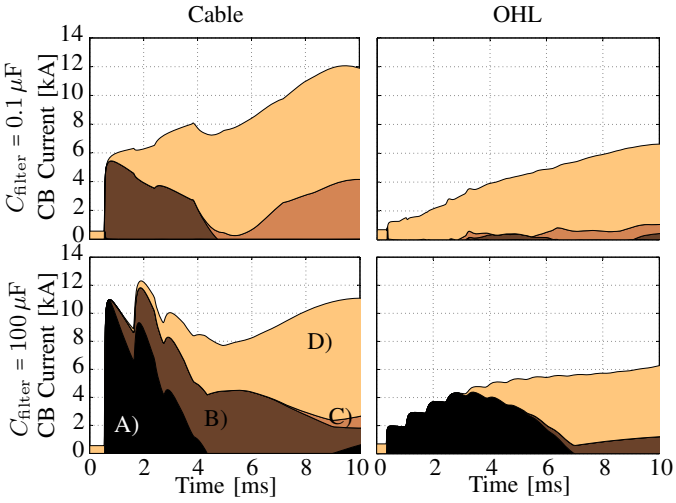

Fig. 6. Fault current contributions: (A) DC capacitor, (B) adjacent feeder cable, (C) AC infeed at terminal 3, (D) AC infeed at terminal 1

As shown in Fig. 5, the fault current in the CB increases over time due to the increasing contribution of the AC networks at terminals 1 and 3 given the SCR of 20 at both PCCs. This results in higher breaking currents for slower CBs. The size of the DC capacitor, however, has only an impact during the first few milliseconds and, therefore, the maximum values of the prospective fault current in the CB within $2\,$ms for various capacitor sizes between 0.1 and $100\,\mu$F are investigated and depicted in Fig. 7. The height of the bars represents the maximum breaking currents, which a fast hybrid DC CB [11] would have to cope with. In the OHL system (dashed bars), the maximum CB current saturates beyond $50\,\mu$F at around $4\,$kA and the DC capacitor is the only fault current contributor. As the size of the DC capacitor decreases, the contribution of the AC infeed at the closest terminal (terminal 1) increases. For the lowest value of the capacitor, the AC infeed is the sole CB fault current contributor. The maximum CB currents always occur $2\,$ms after fault occurrence, which is the upper limit of the considered time frame in this case.

A distinct pattern can be seen in the cable system (solid bars). Its resulting maximum CB currents within $2\,$ms are higher and, in contrast to the OHL system, the adjacent feeder has a considerable share on the total fault current, particularly for the smallest capacitor size and sizes above $60\,\mu$F. Unlike in

the OHL system, the maximum values of the CB current in a cable system occur earlier than 2 ms, except for the maximum in case of the smallest capacitor size. For capacitors with less than 60 μF, the maximum occurs at 0.5 ms when the first negative surge arrives and the DC capacitor is the main fault current contributor. For larger values of more than 60 μF, the second surge leads to the maximum CB current at 1.5 ms and a large contribution of the adjacent feeder, as well as a small contribution of the slowly increasing AC infeed is visible.

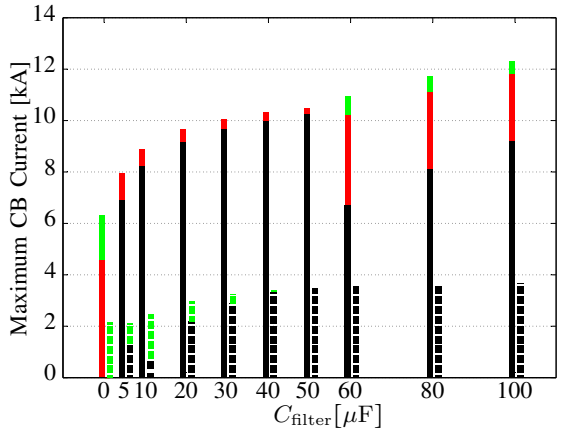

Fig. 7. Maximum CB current within 2 ms in cable (solid bars) and OHL (dashed bars) for various capacitor sizes - black: DC capacitor contribution, red: adjacent feeder contribution, green: AC infeed at terminal 1

D. Influence of Fault Resistance

To investigate the influence of the fault resistance, its value is varied as done with the DC capacitance in the previous paragraph. The DC capacitor is kept constant at 50 μF. Fig. 8 illustrates the CB current development during the first 10 ms for a very small impedance (upper row) and a high-impedance fault (lower row). The level of the CB current decreases in both transmission media for increasing fault resistance. In case of a low fault resistance, the cable exhibits a considerably higher CB current than the OHL, whereas the results of the two transmission technologies do not differ significantly during a high-impedance fault. A small fault resistance results in a high reflection coefficient and yields, therefore, a higher peak of the second capacitor discharge as compared with the high-impedance fault. This effect is particularly visible in the cable system in Fig. 8 (left column). As the reflection coefficient decreases with increasing fault resistance, the transmission coefficient increases accordingly and, consequently, the sudden decrease due to the positive voltage surge at 2.2 ms becomes more accentuated (c.f. Fig. 8 lower left graph).

The maximum CB currents within 2 ms are given in Fig. 9 with solid bars for the cable system and dashed bars for the OHL system for various values of the fault resistance between 0.1 and 100 Ω. For both transmission technologies, the total CB current decreases with increasing fault resistance. The DC capacitor is the only contributor in the cable system for fault resistances above 20 Ω and throughout the variation range in case of OHL lines. The reason for that are again the decreased reflection coefficient for higher fault resistances and, therefore,

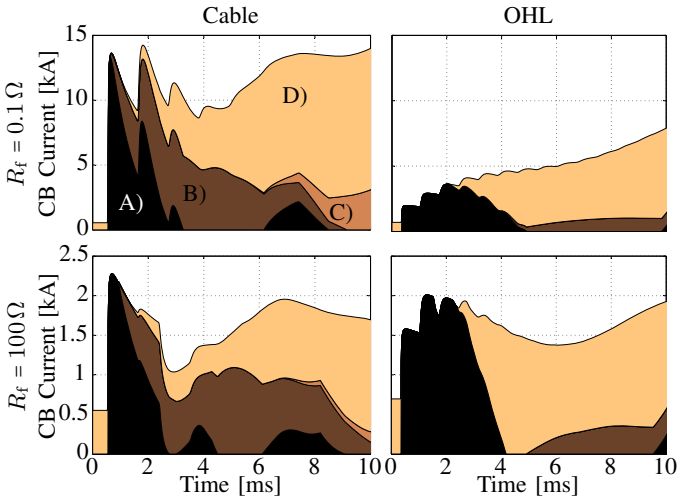

Fig. 8. Fault current contributions: (A) DC capacitor, (B) adjacent feeder cable, (C) AC infeed at terminal 3, (D) AC infeed at terminal 1

a lower second capacitor discharge peak, which, in contrast to the first peak, could also comprise other current contributions than from the filter itself. The maximum values of the CB current in cables and OHLs converge to the same value for a very high fault resistance as it becomes dominant over the line resistance. The sensitivity of the maximum value on the fault resistance is again smaller in OHL than in cable systems.

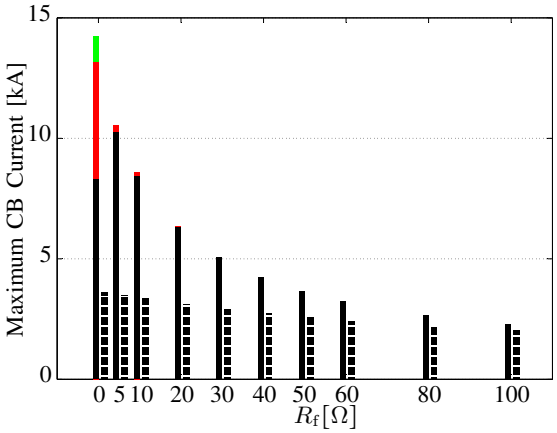

Fig. 9. Maximum CB current within 2 ms in cable (solid bars) and OHL (dashed bars) for various fault resistances - black: DC capacitor contribution, red: adjacent feeder contribution, green: AC infeed at terminal 1

E. Influence of AC SCR

A variation of the SCR of the AC system at the PCCs has no impact on the first, capacitive discharge dominated period up to 5 ms as depicted in Fig. 10. It has, however, a considerable influence on the level of the steady-state short-circuit current in the CB, when the AC infeed is the main contributor. An increase of the SCR affects OHL and cable systems similarly. The additional increase of the fault current due to an increase in the SCR becomes lower towards higher values of the SCR.

V. Conclusion

In this paper, the fault current through a DC CB has been broken down into the individual contributions of the fault

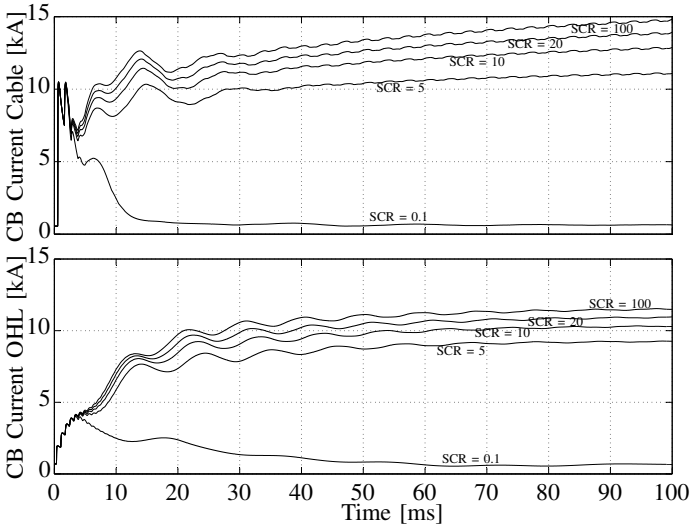

Fig. 10. Fault current in the CB as function of the AC SCR

current feeding components and the dependencies of each contributor on key parameters. The results have shown that the filter and line capacitance discharges are the dominant contributors in the first $10\,\mathrm{ms}$, during which the cable and OHL show distinct discharge patterns. The cables exhibit larger DC capacitor and cable capacitance contributions compared with the OHL due to lower damping (lower R) and higher cable capacitance, respectively. Smaller capacitor discharge peaks are seen in OHL connections, but with a higher frequency given the higher propagation speed. After $10\,\mathrm{ms}$, the AC infeeds at terminals 1 and 3 are exclusively present and the OHL system yields a slightly lower fault current level due to the higher resistivity compared with the cable.

The CB fault current in a cable system has demonstrated high sensitivity to a change of the DC capacitor size and the fault resistance, whereas the influence of these parameters is negligible in OHL systems. An increase in the SCR of the adjacent AC networks at the PCC affects only the steady-state fault current and shows a similar impact on both transmission technologies.

VI. References

[1] D. van Hertem and M. Ghandhari, "Multi-terminal VSC HVDC for the European supergrid: Obstacles," *Renewable and Sustainable Energy Reviews*, vol. 14, no. 9, pp. 3156–3163, 2010.

[2] D. Jovcic, D. van Hertem, K. Linden, J.-P. Taisne, and W. Grieshaber, "Feasibility of DC Transmission Networks," in *Proc. IEEE ISGT Europe*, Manchester, UK, Dec. 2011, pp. 1–8.

[3] Friends of the Supergrid FOSG WG2. (2012, Mar.) Roadmap to the Supergrid Technologies. Final Report. [Online]. Available: http://www.friendsofthesupergrid.eu

[4] OffshoreGrid. (2011, Oct.) Offshore Electricity Grid Infrastructure in Europe. Final Report. [Online]. Available: http://www.offshoregrid.eu

[5] Greenpeace and 3E. (2008, Sep.) A North Sea Electricity Grid Revolution. [Online]. Available: http://www.greenpeace.org

[6] Atlantic Wind Connection. (2012) The Atlantic Wind Connection: A Bold Plan That Makes Sense. Brochure. [Online]. Available: www.atlanticwindconnection.com

[7] Desertec Foundation. (2009, Feb.) Clean Power From Deserts. White Book. [Online]. Available: http://www.desertec.org

[8] L. Tang and B.-T. Ooi, "Locating and isolating DC faults in multiterminal DC systems," *IEEE Trans. Power Del.*, vol. 22, no. 3, pp. 1877–1884, 2007.

[9] W. Long, J. Reeve, J. McNichol, R. Harrison, and D. Fletcher, "Consideration for implementing multiterminal DC systems," *IEEE Trans. Power App. Syst.*, vol. PAS-104, no. 9, pp. 2521–2530, 1985.

[10] C. M. Franck, "HVDC Circuit Breakers: A Review Identifying Future Research Needs," *IEEE Trans. Power Del.*, vol. 26, no. 2, pp. 998–1007, 2011.

[11] J. Haefner and B. Jacobson, "Proactive Hybrid HVDC Breakers - A key innovation for reliable HVDC grids," in *Proc. CIGRE Symposium*, Bologna, Italy, Sep. 2011.

[12] M. K. Bucher, M. M. Walter, M. Pfeiffer, and C. M. Franck, "Options for Ground Fault Clearance in HVDC Offshore Networks," in *Proc. IEEE Energy Conversion Congress and Exposition (ECCE)*, Raleigh, USA, Sep. 2012.

[13] M. K. Bucher and C. M. Franck, "Contribution of Fault Current Sources in Multi-Terminal HVDC Cable Networks," *IEEE Trans. Power Del.*, 2012, submitted for review.

[14] J. Candelaria and J.-D. Park, "VSC-HVDC system protection: A review of current methods," in *Proc. IEEE Power Systems Conference and Exposition (PSCE)*, Phoenix, USA, Mar. 2011, pp. 1–7.

[15] J. Yang, J. Fletcher, and J. O'Reilly, "Short-Circuit and Ground Fault Analysis and Location in VSC-based DC Network Cables," *IEEE Trans. Ind. Electron.*, vol. 59, no. 10, pp. 3827–3837, 2012.

[16] T. Worzyk, Ed., *Submarine Power Cables: Design, Installation, Repair, Environmental Aspects*. Springer Publishing Company, 2009.

[17] J. Wang, A. C. Liew, and M. Darveniza, "Extension of dynamic model of impulse behavior of concentrated grounds at high currents," *IEEE Trans. Power Del.*, vol. 20, no. 3, pp. 2160–2165, 2005.

[18] E. W. Kimbark, "Transient Overvoltages Caused by Monopolar Ground Fault on Bipolar DC Line: Theory and Simulation," *IEEE Trans. Power App. Syst.*, vol. PAS-89, no. 4, pp. 584–592, 1970.

[19] N. G. Hingorani, "Transient Overvoltage on a Bipolar HVDC Overhead Line Caused by DC Line Faults," *IEEE Trans. Power App. Syst.*, vol. PAS-89, no. 4, pp. 592–610, 1970.

[20] B. R. Andersen, L. Xu, P. J. Horton, and P. Cartwright, "Topologies for VSC transmission," *Power Engineering Journal*, vol. 16, no. 3, pp. 142–150, 2002.

[21] R. Marquardt, "Modular Multilevel Converter: An universal concept for HVDC-Networks and extended DC-Bus-applications," in *Proc. IEEE IPEC*, Sapporo, Japan, Jun. 2010, pp. 502–507.

[22] J. Arrillaga, Y. H. Liu, N. R. Watson, and N. J. Murray, Eds., *Self-Commutating Converters for High Power Applications*. Wiley, 2009.

[23] M. P. Bahrman and B. K. Johnson, "The ABCs of HVDC transmission technologies," *IEEE Power Energy Mag.*, vol. 5, no. 2, pp. 32–44, 2007.

[24] G. Miano and A. Maffucci, Eds., *Transmission lines and lumped circuits*. Academic Press, 2001.

[25] H. W. Dommel, "Digital Computer Solution of Electromagnetic Transients in Single-and Multiphase Networks," *IEEE Trans. Power App. Syst.*, vol. PAS-88, no. 4, pp. 388–399, 1969.

[26] J. Yang, J. Fletcher, and J. O'Reilly, "Multiterminal DC Wind Farm Collection Grid Internal Fault Analysis and Protection Design," *IEEE Trans. Power Del.*, vol. 25, no. 4, pp. 2308–2318, 2010.

[27] L. Colla, S. Lauria, and F. Palone, "Short Circuit and Induced Voltage Transient Study on a Planned 1000 MW HVDC-VSC Cable Link," in *Proc. IPST'11*, Delft, The Netherlands, Jun. 2011.

[28] S. Eicher, M. Rahimo, E. Tsyplakov, D. Schneider, A. Kopta, U. Schlapbach, and E. Carroll, "4.5kV press pack IGBT designed for ruggedness and reliability," in *Proc. IEEE Industry Applications Conference*, vol. 3, Oct. 2004, pp. 1534–1539.

[29] L. Ronström, M. Hoffstein, R. Pajo, and M. Lahtinen, "The Estlink HVDC light transmission system," in *Proc. CIGRE Regional Meeting on Security and Reliability of Electric Power Systems*, Tallinn, Estonia, Jun. 2007.

[30] ABB High Voltage Cables. (2006, Oct.) HVDC Light Cables - Submarine and land power cables. [Online]. Available: http://library.abb.com

[31] F. Mura, C. Meyer, and R. W. De Doncker, "Stability Analysis of High-Power DC Grids," *IEEE Trans. Ind. Appl.*, vol. 46, no. 2, pp. 584–592, 2010.

[32] International Electrotechnical Commission (IEC), "Overhead electrical conductors - Calculation methods for stranded bare conductors," Tech. Rep. IEC TR 61597, 1995.

[33] Electrical Power Research Institute (EPRI), "HVDC Transmission Line Reference Book," Final Report EPRI TR-102764, Sep. 1993.